JOURNAL OF GEOPHYSICAL RESEARCH: OCEANS, VOL. 118, 4673–4688, doi:10.1002/jgrc.20306, 2013

Bathymetry correction using an adjoint component of a coupled nearshore wave-circulation model: Tests with synthetic velocity data

Alexander L. Kurapov[1] and H. Tuba Özkan-Haller[1]

Received 19 December 2012; revised 1 July 2013; accepted 6 July 2013; published 20 September 2013.

[1] The impact of assimilation of wave-averaged flow velocities on the bathymetric correction is studied in tests with synthetic (model-generated) data using tangent-linear and adjoint components of a one-way coupled nearshore wave-circulation model. Weakly and strongly nonlinear regimes are considered, featuring energetic unsteady along-beach flows responding to time-independent wave-averaged forcing due to breaking waves. It is found that assimilation of time-averaged velocities on a regular grid (mimicking an array of remotely sensed data) provides sensible corrections to bathymetry. Even though the wave data are not assimilated, flow velocity assimilation utilizes adjoint components of both the circulation and wave models. The representer formalism allows separating contributions of these two components to the bathymetric correction. In a test case considered, involving a beach with an alongshore varying bar, the adjoint wave model contribution was mainly to determine the cross-shore position of the bar crest. The adjoint circulation model provided an additional contribution, mostly adding to alongshore variability in the shape of the bar. The array mode analysis reveals that there are very few modes that can be effectively corrected, given the assumed data error level. Bathymetry perturbations associated with these modes are a mixture of near-coast intensified modes as well as modes extending their influence to deep water (along the background wave characteristics). Additional tests show the utility of different observational arrays in providing the bathymetric correction.

Citation: Kurapov, A. L., and H. T.Özkan-Haller (2013), Bathymetry correction using an adjoint component of a coupled nearshore wave-circulation model: Tests with synthetic velocity data, *J. Geophys. Res. Oceans.*, *118*, 4673–4688, doi:10.1002/jgrc.20306.

1. Introduction

[2] In the nearshore surf zone, knowledge of accurate bathymetry $h(x,y)$ is crucial in many applications, including wave and circulation forecasting and beach erosion monitoring. In response to storms, sand bars and other bathymetric irregularities can be formed, modified, or moved rapidly offshore, sometimes over the span of a day [*Gallagher et al*., 1998]. Frequent high-resolution bathymetric surveys are difficult given harsh surf zone conditions as well as logistical constraints. Inversion of remotely sensed observations of oceanic variables that are sensitive to bathymetry (including currents, wave setup, celerity, dissipation, etc.) can provide an opportunity to obtain estimates of bathymetric changes without direct surveys. As an example, the Beach Wizard system [*van Dongeren et al*., 2008] utilizes estimates of wave celerity, wave dissipation, and intertidal bathymetry (derived from optical or radar observations of the nearshore ocean over an extended period of time) to correct bathymetry locally at points where data are available. The prior estimates of the observed variables are obtained from a numerical wave and circulation model, and a sequential assimilation scheme is devised to constrain bathymetry. This system can assimilate observations of variables that can be expressed in mathematical terms as analytical differentiable functions depending locally on h. Similarly, the c-Bathy algorithm [*Holman et al.,* 2013] provides estimates of bathymetry using wave celerity properties derived from the optical image analysis and local inversion of the wave dispersion relation.

[3] Not every observed oceanic variable sensitive to h can be written as a local analytical function of h. For instance, estimates of wave-averaged currents can be obtained from microwave radar imagery [*Farquharson et al*., 2005] or feature tracking using a sequence of optical images [*Chickadel et al*., 2003]. These currents are influenced by both local bathymetry and bathymetric variability at a distance. For example, bathymetry errors at some distance from the coast can affect estimates of shoreward wave propagation, resulting in erroneous estimates of wave breaking, dissipation, and forcing of wave-averaged currents closer to the coast. In addition, bathymetry also enters explicitly into governing equations of the circulation and thus has a direct effect on a wave-averaged flow field. Hence, bathymetry estimation using observed nearshore currents requires a method that can account for both local

[1]College of Earth, Ocean, and Atmospheric Sciences, Oregon State University, Corvallis, Oregon, USA.

Corresponding author: A. L. Kurapov, College of Oceanic and Atmospheric Sciences, Oregon State University, 104 COAS Admin. Bldg., Corvallis, OR 97331-5503, USA. (kurapov@coas.oregonstate.edu)

2169-9275/13/10.1002/jgrc.20306

and nonlocal dependence on h and utilizes both wave and circulation models.

[4] Some data assimilation methods [*Bennett et al*., 2002; *Evensen*, 2007] are designed to find ocean state estimates that fit the model and the data in a least squares sense. These methods use model error covariances (computed or specified a priori) to provide interpolation and filtering of sparse data sets and to correct model inputs (including in our case bathymetry) at the locations where data are not available. The model error (and correction) is propagated in space and time using the model dynamics, e.g., traveling as waves or advected by currents. *Wilson et al*. [2010] made a step in this direction by assimilating in situ velocity observations and correcting bathymetry, using an ensemble approach to compute model error covariances [*Evensen*, 2007]. An ensemble of bathymetries was generated using empirical orthogonal functions (EOFs) of the bathymetry time series from a series of surveys in the study region. An ensemble of model solutions was obtained using this bathymetry ensemble. From these, the velocity-bathymetry error covariance matrix was obtained, which was used to form a transfer function between the velocity model-observation difference and the bathymetry correction. This method was also later applied in a river setting [*Wilson and Özkan-Haller*, 2012].

[5] Variational methods [*Bennett*, 2002] are based on an explicit formulation of a cost function, which is a sum of quadratic terms penalizing deviations of the model inputs from their prior estimates and model-data differences, defined over a fixed time interval. In the statistical interpretation of the variational method, under a number of assumptions, the minimizer of the cost function yields the best linear unbiased estimate of the model state. In practical applications, the minimum of the cost function is usually found iteratively, by running repeatedly a linearized version of the dynamical model (a so-called tangent linear (TL) model) and its adjoint (AD) counterpart. Building tangent linear and adjoint models may be a challenging exercise. However, once these are developed, variational methods can provide advantages, including: (i) a very clear and explicit formulation of statistical hypotheses about errors in model inputs (including bathymetry), (ii) ability to show error propagation in the model in space and time, e.g., in the spatiotemporal structures of so-called representer functions [*Chua and Bennett*, 2001; *Kurapov et al*., 2003, 2011], and (iii) ability to explore covariability of model input and output errors. They also allow avoiding some of the problems of ensemble methods, including insufficient ensemble sizes, erroneous long-tail model correlations, and the ensemble spread reduction, which would require sequential ad hoc rescaling [*Hamill et al*., 2001]. In the context of our study, the variational formalism will allow us to separate contributions of the wave and circulation models to the bathymetry correction.

[6] Among the contributions utilizing the variational approach with nearshore models, *Feddersen et al*. [2004] tested the method with an alongshore uniform surf zone model. They assimilated in situ observations of pressure and velocities and included bottom friction as one of the corrected variables (but they did not correct h). *Kurapov et al*. [2007] developed TL and AD components of a shallow-water nearshore circulation model and utilized these to demonstrate that variational assimilation can work over extended time windows in strongly nonlinear flow regimes, where the alongshore currents become unstable and eddies are shed. In that study, the dynamics and wave forcing formulation were borrowed from *Slinn et al*. [2000]. The assimilation system was utilized with synthetic (model-generated) velocity data and provided corrections to initial conditions and the circulation model forcing. Bathymetry or offshore wave conditions were not included as control parameters, and the TL and AD components of the wave model were not developed. More recently, *Veeramony et al*. [2010], developed an adjoint component of the nearshore spectral wave model SWAN. They assimilated observed two-dimensional wave spectra to correct boundary conditions of the wave model. However, again, h was not corrected.

[7] In the present manuscript, we will explore opportunities that variational assimilation may offer correcting h in a coupled wave-circulation model. The adjoint component of the model, which provides sensitivity to bathymetry, will be described in section 2. The model is similar to that of *Kurapov et al*. [2007] and only includes one-way coupling. So, the incident wave field is allowed to force nearshore currents; however, the resulting circulation does not affect the incident wave field. We run a series of assimilation experiments with synthetic (model-generated) data and demonstrate the impact of assimilation of velocities to correct errors in bathymetry (section 3). Wave data are not assimilated in our tests here and we focus only on the role played by flow velocity data via both circulation and wave model adjoint components. Compared to other assimilation studies mentioned above, which considered steady flows, we consider weakly and strongly nonlinear regimes, where alongshore flows are unsteady (equilibrated waves or aperiodic eddy-shedding) in response to steady wave-averaged forcing. Analyses of representer functions and array modes (section 4) are utilized to help understand the relative contributions of the wave and circulation model components to the bathymetry correction.

2. Model Setup

[8] The model setup repeats that in *Kurapov et al*. [2007]. Results discussed in this paper are obtained in a domain extending 256 m in the alongshore and 512 m in the offshore direction (Figure 1). The coastline is straight. Boundary conditions are periodic in the alongshore direction. The model resolution is 2 m. A Cartesian coordinate system is introduced with x directed alongshore and y directed offshore. Over the modeling time intervals considered here, the mean water level is assumed to be constant. No wetting-drying is allowed, which is a common assumption for models based on wave-averaged equations [e.g., *Svendsen*, 2006; *Slinn et al*., 2000; *Özkan-Haller and Li*, 2003]. The minimum depth of 0.08 m is set along the coastline.

[9] Figure 1a shows the true bathymetry in the twin experiments, which is identical to that in *Kurapov et al*. [2007]. It has the bar centered at $y = 80$ m. The bar height varies in the alongshore direction. The prior bathymetry (Figure 1b) has the bar displaced offshore by 20 m. Its shape and height are almost uniform in the alongshore

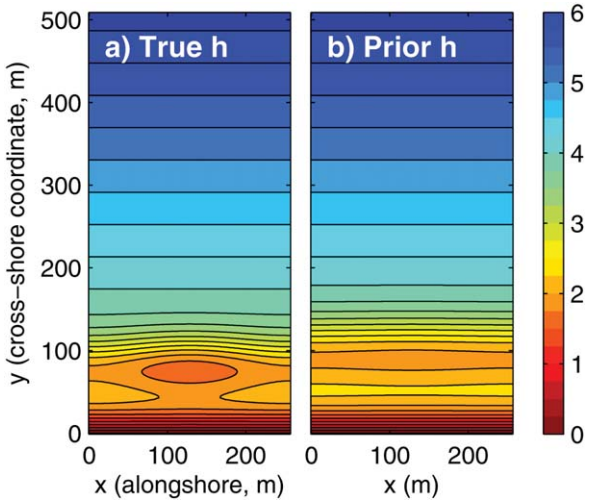

Figure 1. Model bathymetry in twin experiments: (a) true and (b) prior. Black contours are every 0.5 m.

direction (slight nonuniformity is allowed to excite alongshore variability and instabilities in currents). In twin experiments, we will run the nonlinear coupled model both with the true and prior bathymetries. The velocity values from the case with the true bathymetry will be assimilated in the model using the prior bathymetry, and an attempt to correct h will be made.

[10] The diagram in Figure 2a shows information flow in the nonlinear coupled model. Inputs to the wave model component (WAVE) include bathymetry $h(x,y)$ and the incoming wave parameters in deep water (the latter are kept constant in our study and are not shown in the diagram). In all experiments below, similarly to *Kurapov et al.* [2007], we assume that narrow-banded waves are incident at the offshore boundary at an angle of 135°, measured in the clockwise direction from the y axis. The peak wave period is at $T_p = 8$ s. The root mean square (RMS) wave height in the deep water is $H_{rms} = 0.7$ m. The wave model [*Slinn et al.*, 2000; *Özkan-Haller and Li*, 2003] yields fields of two components of the wave vector k and l (in the directions x and y, respectively), wave energy E, wave dissipation ϵ, and also forcing of the circulation model $\boldsymbol{f} = (f_X, f_Y)$, which is obtained as the linear combination of derivatives of the components of the radiation stress tensor (see Appendix A for the wave model equations).

[11] The nonlinear circulation model (denoted CIRC in Figure 2a) is based on the shallow-water equations with biharmonic horizontal dissipation and linear bottom drag [*Kurapov et al.*, 2007]:

$$\frac{\partial \zeta}{\partial t} + \frac{\partial (Du)}{\partial x} + \frac{\partial (Dv)}{\partial y} = 0 \tag{1}$$

$$\frac{\partial (Du)}{\partial t} + \frac{\partial (Duu)}{\partial x} + \frac{\partial (Dvu)}{\partial y} = -gD\frac{\partial \zeta}{\partial x} + f_X - ru - a\nabla^2\left(h\nabla^2 u\right) \tag{2}$$

$$\frac{\partial (Dv)}{\partial t} + \frac{\partial (Duv)}{\partial x} + \frac{\partial (Dvv)}{\partial y} = -gD\frac{\partial \zeta}{\partial y} + f_Y - rv - a\nabla^2\left(h\nabla^2 v\right) \tag{3}$$

where ζ is the sea surface height, u and v are two orthogonal components of depth-averaged velocity, in the directions x and y respectively, $D(x,y,t) = \zeta(x,y,t) + h(x,y)$, and $a = 1.25$ m^4 s^{-1}. Inputs to the circulation model (see Figure 2a) include forcing computed by the wave model $\boldsymbol{f} = (f_X, f_Y)$, bathymetry $h(x,y)$, and the vector of initial conditions $\boldsymbol{u}(0)$ (which combines elements of ζ, u, and v).

[12] The response of the circulation model to the time-invariant (f_X, f_Y) depends on the value of the bottom drag coefficient r. For large values, the system started from rest would equilibrate to a steady flow. For small r, the alongshore current can become unstable. Two cases will be considered in this manuscript, similarly to *Kurapov et al.* [2007]. In the first case $r = 0.004$ m s^{-1}, and the flow regime is weakly nonlinear. After a ~1 h spin-up period, the flow, started from rest, will achieve an equilibrated wave regime, with the currents meandering and flowing in the direction of negative x. Several snapshots of velocity and vorticity $\frac{\partial v}{\partial x} - \frac{\partial u}{\partial y}$ corresponding to this regime are shown in Figure 3 (top). In the second case $r = 0.002$ m s^{-1}, and the flow regime is strongly nonlinear. After a ~1 h spin-up period, the area-averaged kinetic energy of the system levels off and begins to vary near a certain level, but the solution

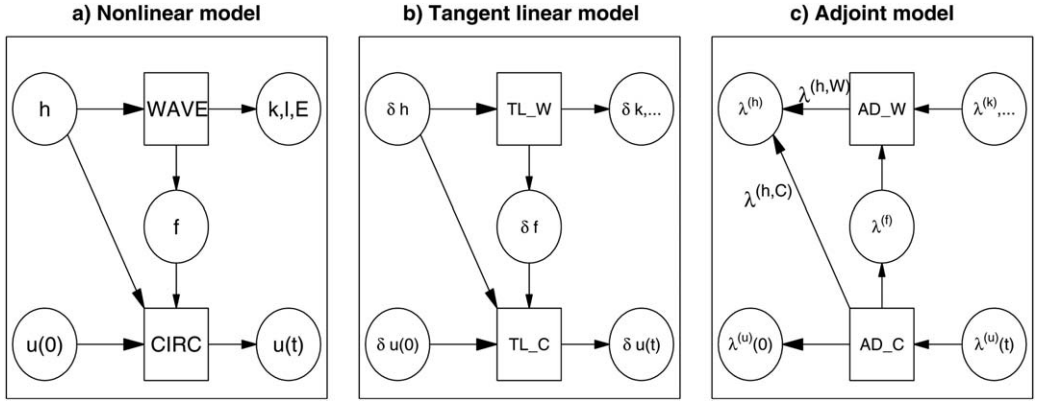

Figure 2. The schematics of the coupled model components: (a) nonlinear, (b) tangent linear (information flow is similar to the nonlinear model), and (c) adjoint (information flow is reversed compared to the nonlinear and tangent linear models).

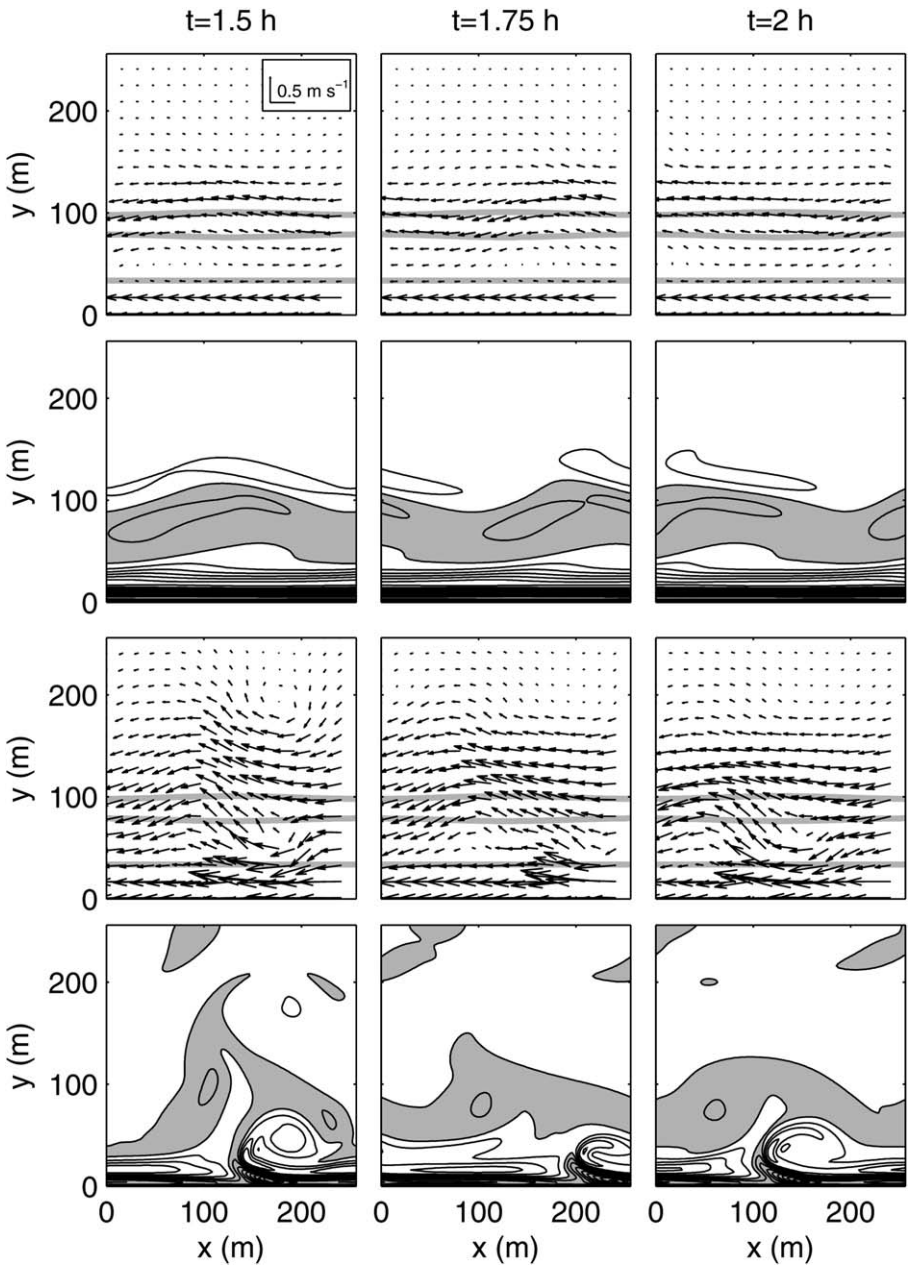

Figure 3. Snapshots of velocity (vectors) and vorticity (contours) at three time instances (left to right: 1.5, 1.75, and 2 h since the start from rest). Upper plots (rows 1 and 2): $r = 0.004$ m/s; lower plots (rows 3 and 4): $r = 0.002$ m/s. Half-tone contours in the background of the velocity plots are $h = 2$ m (showing the location of the bar between 70 and 100 m offshore); vorticity contours are every 0.01 s^{-1} (top)/0.02 s^{-1} (bottom), with positive values shaded.

is aperiodic, affected by the generation of energetic eddies (Figure 3, bottom).

[13] The tangent linear (TL) model describes evolution of a small perturbation to the model inputs with respect to a given nonlinear model solution (background model state). The information flow in the TL coupled model (Figure 2b) is similar to that in the nonlinear model. The linearized coupled model has been built using wave and circulation model components (TL_W and TL_C). The TL computer codes have been written by hand using recipes for line-by-line code differentiation [*Guiring and Kaminski*, 1998]. To build TL_C, we modified the shallow-water model code used in *Kurapov et al.* [2007] to include perturbation in h. This modification was relatively easy since the original code already had dependency on perturbation of the total depth $D(x, y, t) = \zeta + h$. Specifically, in the original code, we had $\delta D = \delta\zeta$, where δ denotes the perturbation variable. In the new code, $\delta D = \delta\zeta + \delta h$, where the bathymetry perturbation δh is provided as the input to the TL model.

[14] The background solution is provided into TL_C (and its adjoint counterpart AD_C) as a series of instantaneous fields from the nonlinear circulation model saved at

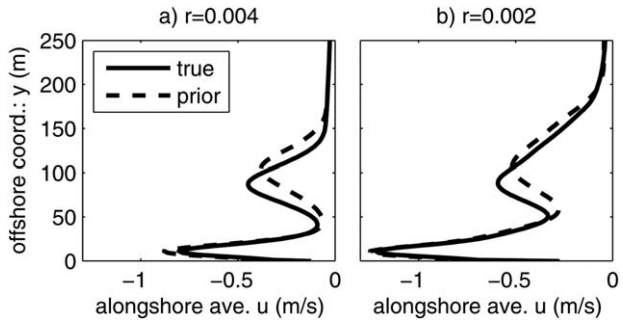

Figure 4. The alongshore current averaged in space in the alongshore direction and in time (over the interval of (1, 2) h); the solid (dashed) line corresponds to the current over the true (prior) bathymetry: (a) $r = 0.004$ m s^{-1} and (b) $r = 0.002$ m s^{-1}.

specified time intervals (every 30 s in the weakly nonlinear case and 15 s in the strongly nonlinear case). Then the TL and AD circulation models determine background circulation fields at every time step by linear interpolation between the saved snapshots.

[15] Model TL_W had to be newly developed. To allow line-by-line code differentiation, the original nonlinear wave model had to be modified in the following respect. *Slinn et al*. [2000] solve wave propagation equations by integration along wave characteristics. The resulting k and l are found along the wave characteristics and then interpolated on the regular Cartesian grid. To avoid difficulties linearizing this two-dimensional interpolation algorithm, we replaced integration along the wave characteristics by solving the following equation on the regular grid:

$$curl(k,l) = \frac{\partial l}{\partial x} - \frac{\partial k}{\partial y} = 0. \tag{4}$$

[16] This equation expresses conservation of wave crests [*Dean and Dalrymple*, 1991]. It can be integrated numerically from the offshore boundary toward the coast, e.g., using a fourth-order Runge-Kutta method, along lines $y = \text{const}$ of the original rectangular grid. In all other aspects (dispersion relation, wave energy equation, and parameterization of dissipation, see Appendix A) the wave model is easily differentiable.

[17] Note that δh influences the output of TL_C in two ways (see Figure 1b). The first is direct, since h enters equations (1)–(3) via D; the second is via the wave model TL_W, providing forcing due to the radiation stress divergence.

[18] Since a discrete numerical model is utilized, a TL model implementation can be viewed as the result of matrix-vector multiplication, $\delta\alpha = [TL]\delta\phi$, where $\delta\phi$ and $\delta\alpha$ are the vectors of model inputs and outputs, respectively. As a part of code testing, we have verified that the result of TL_W implementation, $[TL_W]\delta\phi$, tends to the difference of two nonlinear models, $[NL_W](\phi + \delta\phi\ ) - [NL_W](\phi)$, as the magnitude of $\delta\phi$ is reduced.

[19] Following the same matrix-vector interpretation, the AD model can be defined as the matrix transpose of $[TL]$. Of course, we do not store every element of $[TL]$ or its transpose. Instead, the AD model code provides the rule by which the matrix $[AD]$ multiplies an appropriate vector of inputs. It can be built by transposition of the TL code line-by-line (and reversing the order of operators) using recipes from *Guiring and Kaminsky* [1998]. Both the circulation and wave components of the coupled AD model have been tested to guarantee that the matrix-product $Q^T[AD][TL]Q$ (where $Q = [\delta\varphi_1|\delta\varphi_2|\ldots|\delta\varphi_n]$ is a collection of n randomly generated TL model input vectors) is an $n \times n$ symmetric and positive-definite matrix (within machine precision).

[20] In the scheme corresponding to the AD model (Figure 2c) the information flow is reversed compared to the TL model. In this scheme, symbols λ with different superscripts denote various components of the input and output vectors. The set of the AD input fields has the same structure as the set of outputs of the TL model. In practice, the AD model is forced by adding impulses to adjoint model variables at observation locations and times (for a more formal explanation, see, e.g., *Kurapov et al*. [2007, 2011]). Observations of the wave properties (such as wave vector components) would provide forcing directly to the wave model component AD_W represented in Figure 2c by $\lambda^{(k)}$ and assimilation of those data types would not require a circulation model component AD_C. Data on currents assimilated in the model provide impulse forcing $\lambda^{(u)}(t)$ to AD_C, which in turn yields fields of sensitivity of the observed circulation variables to initial conditions $\lambda^{(u)}(0)$ and circulation model forcing $\lambda^{(f)}(t)$. The latter provides forcing of the AD_W model component, in addition to $\lambda^{(k)}$. If wave variables are not assimilated, the AD_W will only be forced by $\lambda^{(f)}(t)$. Note that AD_C, the adjoint of the time-stepping circulation model, is run backward in time. Every time step adjoint sensitivity to h is added to $\lambda^{(h,C)}$. Then AD_W (which is integrated from the coast to the offshore boundary) provides additional contribution $\lambda^{(h,W)}$ to yield the total sensitivity of flow velocities to bathymetry $\lambda^{(h)} = \lambda^{(h,C)} + \lambda^{(h,W)}$. We have to stress that $\lambda^{(h,W)}$ should not be confused with the sensitivity due to assimilation of wave variables. Even if only wave-averaged currents are assimilated (as discussed below), bathymetry estimation will require both model components, AD_W and AD_C, and the adjoint sensitivity $\lambda^{(h)}$ includes contributions from terms $\lambda^{(h,C)}$ and $\lambda^{(h,W)}$.

3. Assimilation Experiments

[21] The assimilation system discussed here can in general be used to assimilate any oceanic variables that can be matched to the model output. In particular, estimates of the wave vector components (k,l), or wave celerity, obtained from a sequence of radar or optical images, could be assimilated. The impact of these data types has been demonstrated, e.g., by *van Dongeren et al*. [2008] and *Holman et al.* [2013] using methods based on local inversion. In the adjoint counterpart of a one-way coupled model (see Figure 2c), the information from the wave parameter data does not go through the adjoint circulation model component. Since the focus of this manuscript is on aspects of assimilation with the coupled model, we do not include here examples assimilating wave properties and proceed directly to the case of assimilating currents.

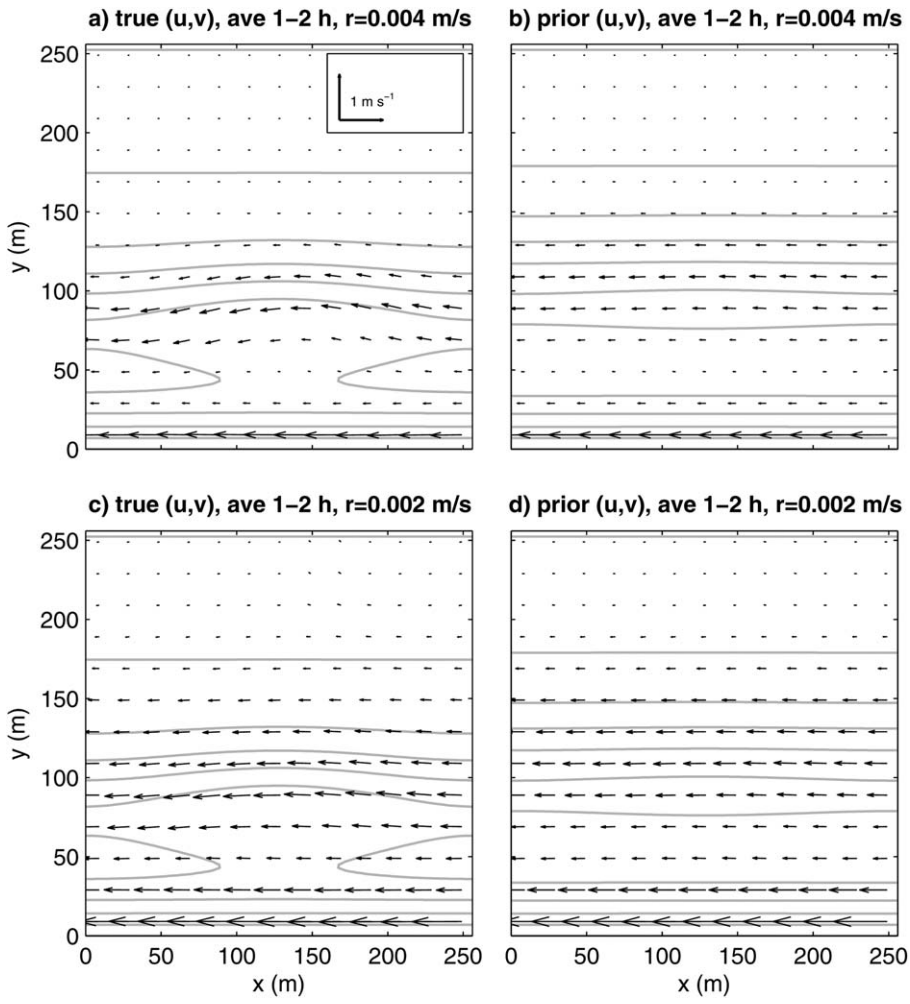

Figure 5. Time-averaged ($t = 1$–2 h) currents shown at every second observational location: (top) the weakly nonlinear case, (bottom) the strongly nonlinear case, (left) the true solution, and (right) the prior solution. Half-tone lines are bathymetry (every 0.5 m).

[22] Model currents are sensitive to the bathymetry details in our case. For instance, Figure 4 shows cross-shore profiles of alongshore currents computed over the true and prior bathymetries, averaged in the alongshore direction and also averaged in time over the interval of (1,2) h since the model was started from rest. In both weakly and strongly nonlinear cases, the largest differences are found in the area of the bar.

[23] In the first series of assimilation tests, data sets are formed by sampling the true model velocities at points of a regular grid in an area extending 256 m offshore. The distance between neighboring data points is 10 m in both the alongshore and cross-shore directions (mimicking a data array from remote sensing; observation locations are shown in Figure 15c).

[24] The variational data assimilation problem for a 2 h spin-up case is considered. The true and prior models are both started from rest. Velocities from the true solution are averaged over the second half of the time interval (1,2) h and sampled at the points of the observational array. Comparisons of the true and prior time-averaged velocity fields sampled at the observation locations show appreciable differences (Figure 5). Differences between the true and prior solutions turn out to be larger in the weakly nonlinear case than the strongly nonlinear case, which can be confirmed by plotting the magnitude of the difference of the time-averaged currents $\sqrt{\left(\overline{u}^{TRUE} - \overline{u}^{PRIOR}\right)^2 + \left(\overline{v}^{TRUE} - \overline{v}^{PRIOR}\right)^2}$, where $\overline{u}$ and $\overline{v}$ correspond to the velocity components averaged over interval $t = (1,2)$ h (Figure 6). In our interpretation, the more energetic flow corresponding to a smaller bottom friction coefficient case is less sensitive to the shape of the bottom.

[25] Before assimilation, random noise is added to the time-averaged synthetic data, with the standard deviation of $\sigma_d = 0.03$ m s^{-1}. Note that this relatively low error level can be attained for 1 h averaged data even if the instantaneous observations are rather noisy (for instance, if the error of the instantaneous data sampled once every minute is temporally uncorrelated and normally distributed with the standard deviation of 0.2 m s^{-1}). The correction to $h(x,y)$ is found by minimizing the cost function as follows:

$$J = \left(h - h^{PRIOR}\right)^T C_h^{-1} \left(h - h^{PRIOR}\right) + \left(d - L\mathbf{u}^{PRIOR}\right)^T C_d^{-1} \left(d - L\mathbf{u}^{PRIOR}\right), \tag{5}$$

subject to the exact model dynamics and exact initial conditions $(\zeta(0) = 0, u(0) = 0, v(0) = 0)$. In (5), h is written

as a vector including bathymetric values at all interior grid points; C_h (x_1, y_1, x, y) is the bathymetric error covariance matrix, with elements depending on the location of grid points (x_1, y_1) and (x, y); d is the vector of all time-averaged observations; u^{PRIOR} is the prior model solution; $L.$ is the operator matching the model solution and the observations (which involves sampling at the data locations and time-averaging of the model output); the superscript ^{T} denotes matrix transpose; and $C_d = \sigma_d^2 I$ is the data error covariance (where I is the unity matrix). The following form is assumed for the bathymetric error covariance:

$$C_h(x_1,y_1,x,y) = \sigma_h^2 \alpha(x_1,y_1)\alpha(x,y) \exp\left[-\frac{(y-y_1)^2}{2l_Y^2}\right] \exp\left[-\frac{1-\cos[q(x-x_1)]}{(ql_X)^2}\right] \quad (6)$$

where

$$\alpha(x,y) = \begin{cases} \sin^2\left[\frac{\pi}{2}\frac{h(x,y)}{h_{\min}}\right], & \text{if } h < h_{\min} \\ 1, & \text{if } h \geq h_{\min} \end{cases} \quad (7)$$

$q = 2\pi/L_X$ and $L_X.$ is the periodic channel length. For given x_1 and y_1, the product of the exponential functions in (6) is a bell-shaped function in x and y. The functional dependence in x conveniently accounts for the domain periodicity [*Ménard*, 2005]. Note that this particular functional form is not influenced by knowledge of the true bathymetry in our case (the cosine function in (6) emerges if ends of a periodic domain are connected and the domain presented as a circle; then the correlation is defined as a Gaussian function of the distance between points on the circle). The scaling function α $(0 \leq \alpha \leq 1)$ in equation (7) is to reduce error standard deviation (and hence the magnitude of the correction) in very shallow water, to possibly avoid drying. The following parameters were used in our experiments: $\sigma_h = 0.05$ m, $h_{min} = 1.5$ m, $l_X = 50$ m, and $l_Y = 20$ m.

[26] The minimizer of equation (7) is obtained with the use of the indirect representer method [*Chua and Bennett*, 2001; *Bennett*, 2002; *Kurapov et al*., 2007, 2011]. Without discussing every detail, we mention here that the original nonlinear optimization problem is linearized with respect to the prior solution and the correction is obtained as an optimal linear combination of representer functions:

$$h^{INVERSE} = h^{PRIOR} + \delta h = h^{PRIOR} + \sum_{k=1}^{K} b_k \delta h_k \quad (8)$$

where δh_k is the bathymetry component of the representer corresponding to the k-th observation, b_k are representer coefficients, and K is the total number of data. Fields δh_k show zones of influence of each velocity observation on the bathymetry. To compute each δh_k, the AD model can be forced with the impulse at the corresponding observational location and time. Since the time-averaged current data are assimilated, a fraction of the impulse is added to the velocity component of the adjoint solution multiple times spread over the period of (1,2) h. The AD model returns adjoint sensitivity in the initial conditions $\lambda_k^{(u)}(0)$ and bathymetry $\lambda_k^{(h)}$, corresponding to the k-th observation. Then $\delta h_k = C_h \lambda_k^{(h)}$. If the coupled TL model is started with δh_k and zero initial condition perturbation (corresponding to the exact initial conditions in our case), the output will be a representer r_k, which would include fields corresponding to each TL model output component (such as wave vector components, wave energy, and the time-varying current fields). Sampling the full set of representers at observation locations and time, we obtain a symmetric and positive-definite representer matrix: $R = L[r_1|\cdots|r_K]$, of size $K \times K$. Then, the optimal set of representer coefficients $b = \{b_k\}$ can be obtained solving the linear algebraic system as follows:

$$(R + C_d)b = d - L\mathbf{u}^{PRIOR} \quad (9)$$

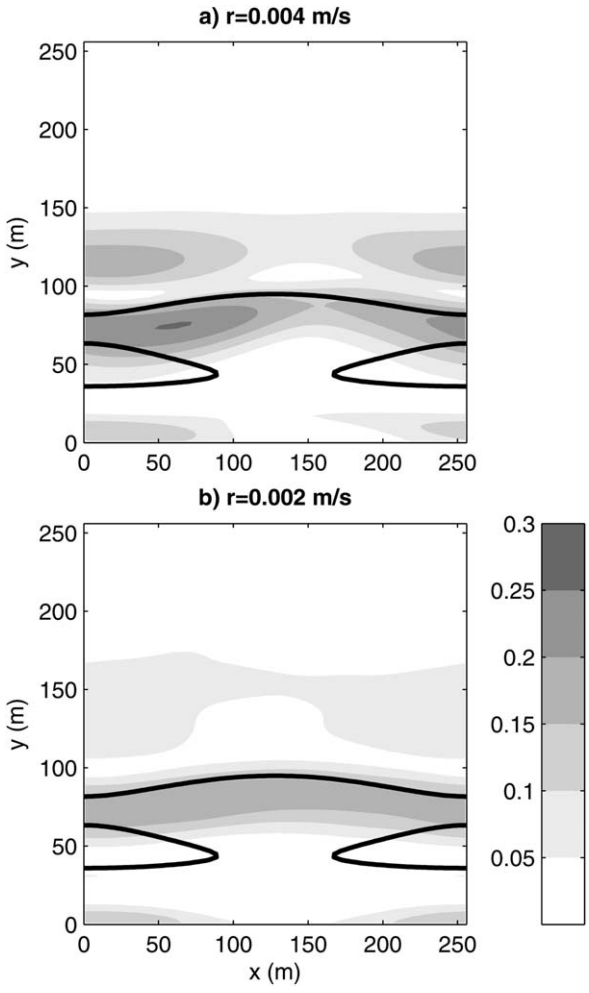

Figure 6. The magnitude of the difference of the true and prior time-averaged velocities $\sqrt{(\overline{u}^{TRUE} - \overline{u}^{PRIOR})^2 + (\overline{v}^{TRUE} - \overline{v}^{PRIOR})^2}$, where $\overline{u}$ and $\overline{v}$ correspond to the velocity components averaged over interval $t = (1, 2)$ h: (a) the weakly nonlinear case and (b) the strongly nonlinear case.

[27] Note that matrix R is generally poorly conditioned (see discussion of the spectrum of R in section 4). A non-zero C_d stabilizes inversion.

[28] In the indirect representer method [see *Bennett*, 2002], which is designed for large data sets, it is not necessary to compute each representer. The initial guess about b is made. The AD system is forced with a linear

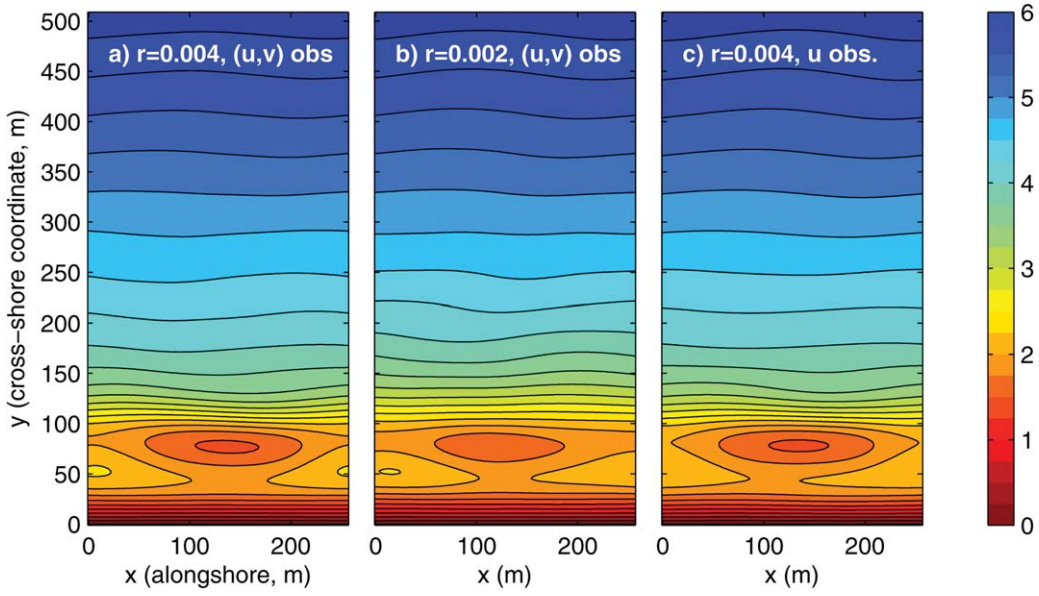

Figure 7. Inverse bathymetry: (a) $r = 0.004$ m s^{-1}, assimilating u and v components, (b) $r = 0.002$ m s^{-1}, assimilating u and v components, and (c) $r = 0.004$ m s^{-1}, assimilating the alongshore (u) component only. The corresponding RMS errors with respect to the true bathymetry are listed in Table 1. For alongshore average bathymetry profiles see Figure 8.

combination of impulse forcings at data locations and times, each scaled by b_k. The bathymetry component of the AD model output is convolved with the covariance C_h, to obtain an estimate of δh. The TL model is then run given δh and the zero initial condition perturbation. The TL model output is sampled at the observation locations, using operator L, and the resulting vector yields the product Rb, which is used in the conjugate gradient method to solve (9) iteratively. This product, the data error covariance, and the prior model-data misfit (the rhs of (9)) are utilized in each iteration to obtain a better estimate of b. This AD-TL cycle is repeated until the following convergence criterion is satisfied:

$$\frac{\|(R + C_d)b - \left(d - L\mathbf{u}^{PRIOR}\right)\|^2}{\|d - L\mathbf{u}^{PRIOR}\|^2} \leq 10^{-3}. \qquad (10)$$

[29] Three tests have been considered. Plots of estimated bathymetries in each test are shown in Figure 7. In the first (Figure 7a), the flow was weakly nonlinear ($r = 0.004$ m s^{-1}) and both velocity components were assimilated at each data point. In the second (Figure 7b), the flow was strongly nonlinear ($r = 0.002$ m s^{-1}) and both velocity components were assimilated. In the third (Figure 7c), the flow was weakly nonlinear ($r = 0.004$ m s^{-1}) and only the alongshore velocity component u was assimilated at each data point, simulating the observational sets that can be obtained from optical imagery [*Chickadel et al.*, 2003]. In every case, the bathymetry is improved qualitatively and also quantitatively in terms of the area-averaged root mean square (RMS) error (Table 1). In every case, the bar is moved toward the shore and is shaped to correspond more closely to the true bathymetry. The displacement in the bar location is best seen in alongshore-averaged bathymetry profiles (Figure 8). In the case of the weakly nonlinear flow, the result assimilating only the u velocity component is as good as that assimilating both velocity components (e.g., compare RMS statistics and Figures 8a and 8c; also see discussion in section 5). In the case of the strongly nonlinear flow (Figure 8b), although the bathymetry is generally improved the slope offshore of the bar is not quite correct.

4. Representer and Array Mode Analysis: Experiments With Different Observational Arrays

[30] In this section, analyses of the h-component of the adjoint sensitivity field $\lambda_k^{(h)}$, the h-component of the representer δh_k, and the correction δh (which is the optimal linear combination of δh_k) are discussed with the goal of understanding relative contributions of the wave and circulation models to the bathymetry correction. The results from the weakly nonlinear case assimilating both components of velocity are used for illustration.

[31] The plots of $\lambda_k^{(h,W)}$ and $\lambda_k^{(h)} = \lambda_k^{(h,W)} + \lambda_k^{(h,C)}$ corresponding to a single observation of the alongshore velocity at a location over the bar are shown in Figure 9. Velocity-bathymetry sensitivity $\lambda_k^{(h)}$ may be interpreted as the model

Table 1. The Bathymetric RMS Error (cm), With Respect to the True Bathymetry, of the Prior and the Three Inverse Estimates Obtained in the Assimilation Tests Using the Observational Array as in Figure 15c

Prior h	19.1
Inverse h, weakly nonlinear flow, (u,v) observations	7.68
Inverse h, strongly nonlinear flow, (u,v) observations	13.7
Inverse h, weakly nonlinear flow, u observations	7.11

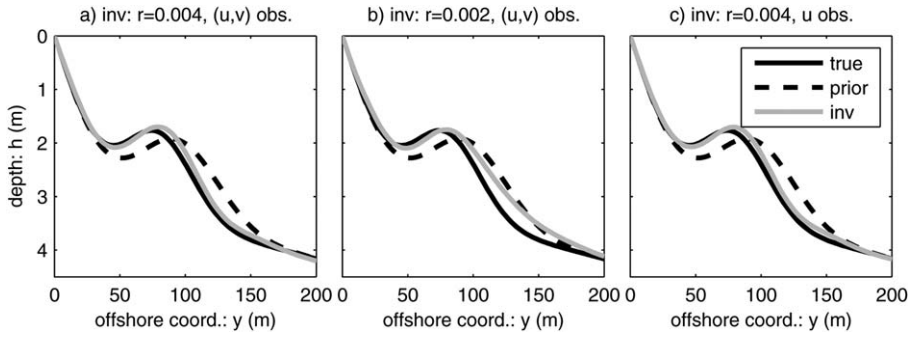

Figure 8. Alongshore average bathymetry profiles, true (solid black), prior (dashed), and inverse (halftone): (a) $r = 0.004$ m s^{-1}, assimilating u and v components; (b) $r = 0.002$ m s^{-1}, assimilating u and v components; (c) $r = 0.004$ m s^{-1}, assimilating the alongshore (u) component only.

error covariance of the bathymetry $h(x,y)$ and the time-averaged velocity component at the observed location under the assumption that bathymetric errors are spatially uncorrelated ($C_h = I$) [see *Bennett*, 2002]. The wave and circulation constituents $\lambda_k^{(h,W)}$ and $\lambda_k^{(h,C)}$ have different spatial structures. The output of the adjoint circulation model $\lambda_k^{(h,C)}$ is nearly singular, showing large sensitivity of the time-averaged velocity to local changes in bathymetry. The singular behavior of the adjoint sensitivity field is a common occurrence in advective transport systems [*Chua and Bennett*, 2001; *Bennett*, 2002]. If the color scale was adjusted, we could also see some influence of the bathymetry along the bar (as the effect of advection by the background current). The alongshore advection also impacts the forcing of the adjoint wave model $\lambda_k^{(f)}$, resulting in enhanced sensitivity along the bar location ($80 < y < 100$ m) in the output of the adjoint wave model $\lambda_k^{(h,W)}$. Also, this field shows sensitivity of the velocity to bathymetry changes farther offshore, in a general direction of the background wave propagation. This pattern could be expected, as errors (corrections) in the bathymetry offshore of the observation location would affect propagation and dissipation of the wave, hence the forcing of the circulation model and the resulting velocity at the observed location.

[32] Applying the covariance C_h to each of the two terms of $\lambda_k^{(h)}$ separately and to the sum, the corresponding fields of δh_k^W are obtained (Figure 10). The singularity at the observation location is smoothed as a result of the covariance implementation. For the selected observation, the structure of the total δh_k is dominated by its wave constituent, although the circulation term provides a nonnegligible contribution in the area over the bar (where its magnitude is about 30% of that of the wave model term). Relative contributions δh_k^W and δh_k^C to the bathymetric correction may depend on the observation location. The covariability pattern along the wave characteristics in deeper water is preserved in both δh_k^W and δh_k. This suggests a potential for correction (or at least an impact) in the deep water area not covered by the data. In our test case, the true and prior

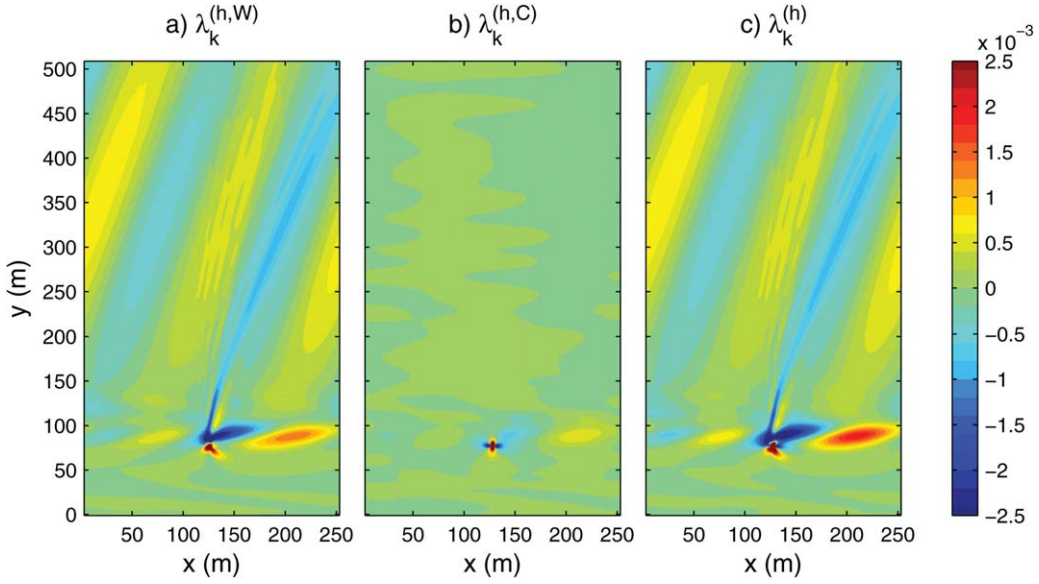

Figure 9. The adjoint bathymetry field corresponding to a single observation, resulting from the adjoint representer computation; units are (m s^{-1}) m^{-1}; the observation location is at the point where the solution is nearly singular: (a) $\lambda_k^{(h,W)}$, (b) $\lambda_k^{(h,C)}$, and (c) $\lambda_k^{(h)} = \lambda_k^{(h,W)} + \lambda_k^{(h,C)}$.

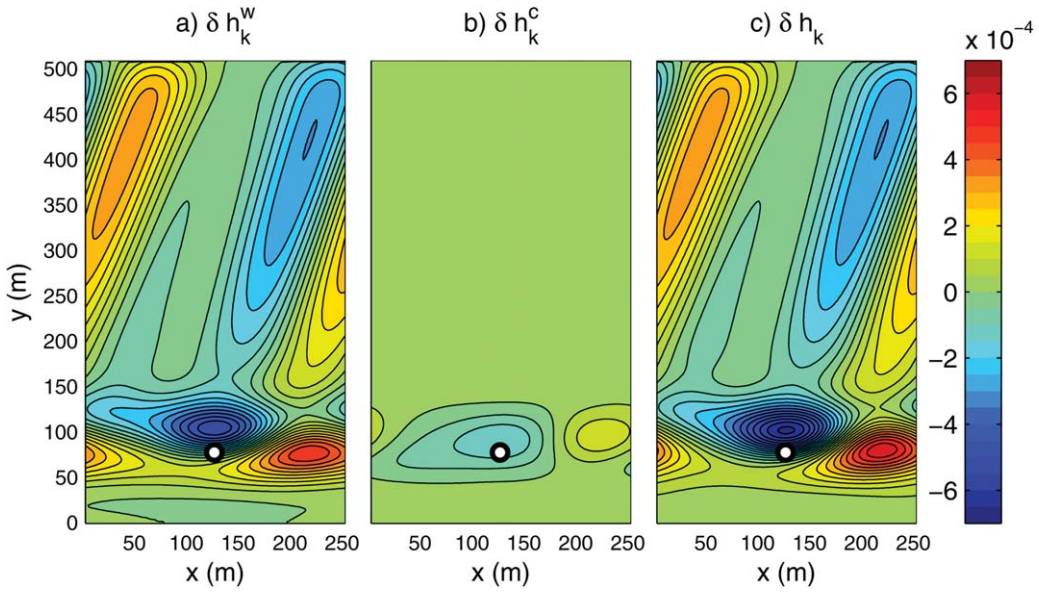

Figure 10. The representer bathymetry components, obtained by applying the prior error covariance C_h to the adjoint fields shown in Figure 9; contours are every 5×10^{-5} m^2 s^{-1}; the observation location is shown as the circle: (a) δh_k^W, (b) δh_k^C, and (c) $\delta h_k = \delta h_k^W + \delta h_k^C$.

bathymetries are very similar far offshore, where a correction would not be needed. Remarkably, despite the fact that the bathymetry error standard deviation $\alpha(x,y)$ (7) is not reduced in deep water, the offshore impacts from each representer nearly cancel in the optimal combination (8) such that the net bathymetric correction is minimal far offshore (although small undulations can still be seen in the inverse bathymetry at $y > 250$ m, see Figure 7).

[33] To understand relative contributions of the circulation and wave adjoint model components to the bathymetry correction given the whole observational array, we will next analyze the optimal linear combinations

$$\delta h_W = \sum_{k=1}^{K} b_k \delta h_k^W, \quad \delta h_C = \sum_{k=1}^{K} b_k \delta h_k^C \tag{11}$$

as well as the total bathymetric correction $\delta h = \delta h_W + \delta h_C$ (the second term on the RHS of (8)) (Figure 11). The term δh_W (Figure 11a) is positive (negative) in the area offshore (onshore) of the prior bar location. This means that the

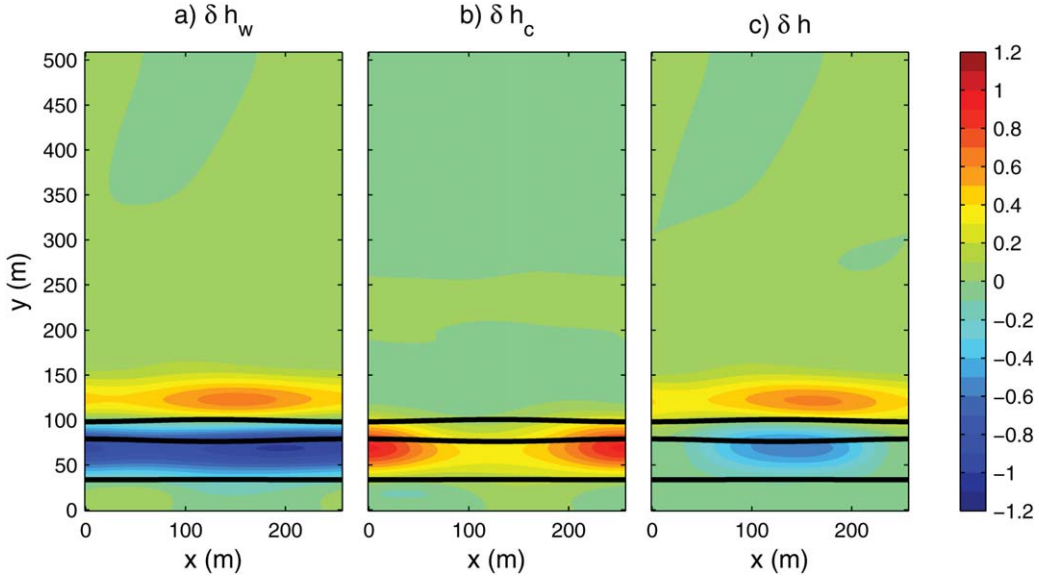

Figure 11. Contributions of the wave and circulation models to the bathymetric correction and the total correction (meters): (a) δh_W, (b) δh_C, and (c) $\delta h = \delta h_W + \delta h_C$. The black lines are the 2 m isobaths in the prior bathymetry (the two lines offshore show the location of the bar). The case is with $r = 0.004$ m/s, assimilating u and v components.

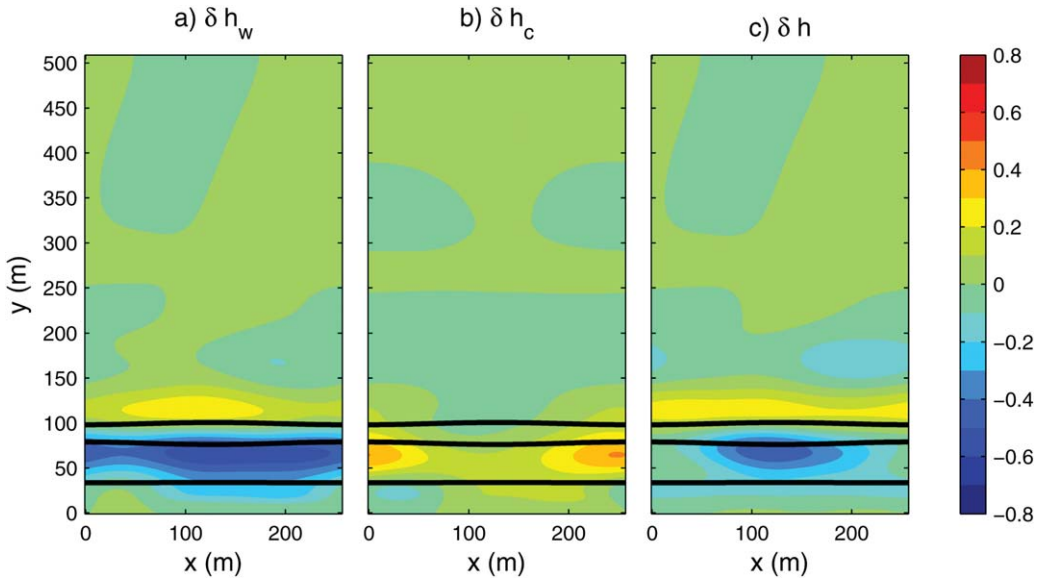

Figure 12. Similar to Figure 11, for the strongly nonlinear case ($r = 0.002$ m^{-1}). Note a different (finer) scale of the color bar.

adjoint wave model contributes to the bathymetric correction mostly by displacing the bar inshore. The term δh_C (Figure 11b), provided directly by the adjoint circulation model, is the largest in the area of the true bar location, additionally deepening the bathymetry at the left and right sides of the bar. Thus, in our case, the two adjoint model components have distinct roles. While AD_W is responsible for displacing the bar, AD_C shapes the bar, varying bathymetry in the alongshore direction. This is consistent with our understanding that the wave properties are more sensitive to the location of the bar than low-amplitude alongshore variability in the bar shape. In turn, time-averaged currents are sensitive to the alongshore variability in the bar shape.

[34] It should be noted that the output of the adjoint wave model δh_W is not independent from the adjoint circulation model. The AD_C component of the coupled assimilation system provides sensitivity of the velocity to the wave model forcing ($\lambda^{(f)}$, see Figure 2c), which is utilized to force AD_W. In broad terms, this sensitivity contains information about where the largest impact of the waves on the circulation can be.

[35] A similar result, showing different spatial patterns in δh_W and δh_C, is obtained in the strongly nonlinear case (Figure 12). The deepening of the slope offshore of the true bar location is not as pronounced as in the weakly nonlinear case, in part because the true-prior velocity difference in the area of the bar is smaller in the strongly nonlinear case (see Figure 6).

[36] The representer method also allows us to perform array mode analysis [*Egbert*, 1997; *Bennett*, 2002; *Kurapov et al.*, 2009] to identify spatial structures that can be corrected most stably given errors in the data. This is illustrated here using the weakly nonlinear case, assimilating both components of velocity. The analysis is based on the eigenvalue decomposition of $R + C_d$. In our case, there are only 1250 observations of the time-averaged u and v, such that computation of all the representers is possible resulting in the full representer matrix. Since $C_d = \sigma_d^2 I$ in our case, we can compute the singular vector decomposition of $R = USU^T$ and rewrite the equation for the optimal representer coefficients (8) as follows:

$$b = U\left(S + \sigma_d^2 I\right)^{-1} U^T \left(d - L\mathbf{u}^{PRIOR}\right). \tag{12}$$

[37] Elements of the vector $U^T d$ are array modes obtained as linear combinations of the original data set, and $U^T L\mathbf{u}^{PRIOR}$ is their model counterpart. Given the prior assumptions about the model input errors (in particular C_h), the diagonal matrix S is the prior covariance of errors in elements of the vector $U^T L\mathbf{u}^{PRIOR}$. The diagonal elements s_k of this matrix yield the expected prior model error variance in each element of $U^T L\mathbf{u}^{PRIOR}$ (Figure 13). The linear combinations for which $s_k > \sigma_d^2$ can be corrected stably (with respect to errors in the data). We find that in our case

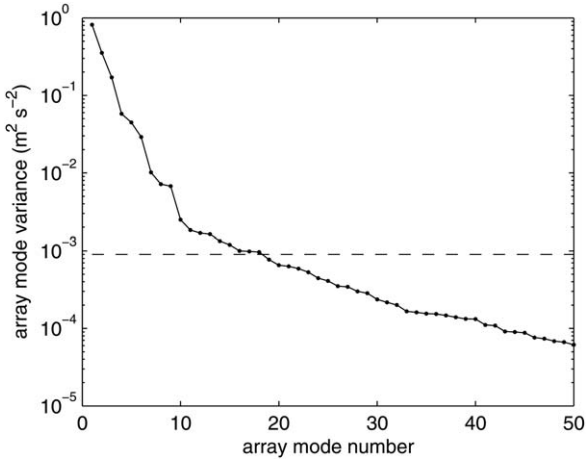

Figure 13. The representer matrix spectrum (variances of the first 50 array modes). The dashed line corresponds to σ_d^2.

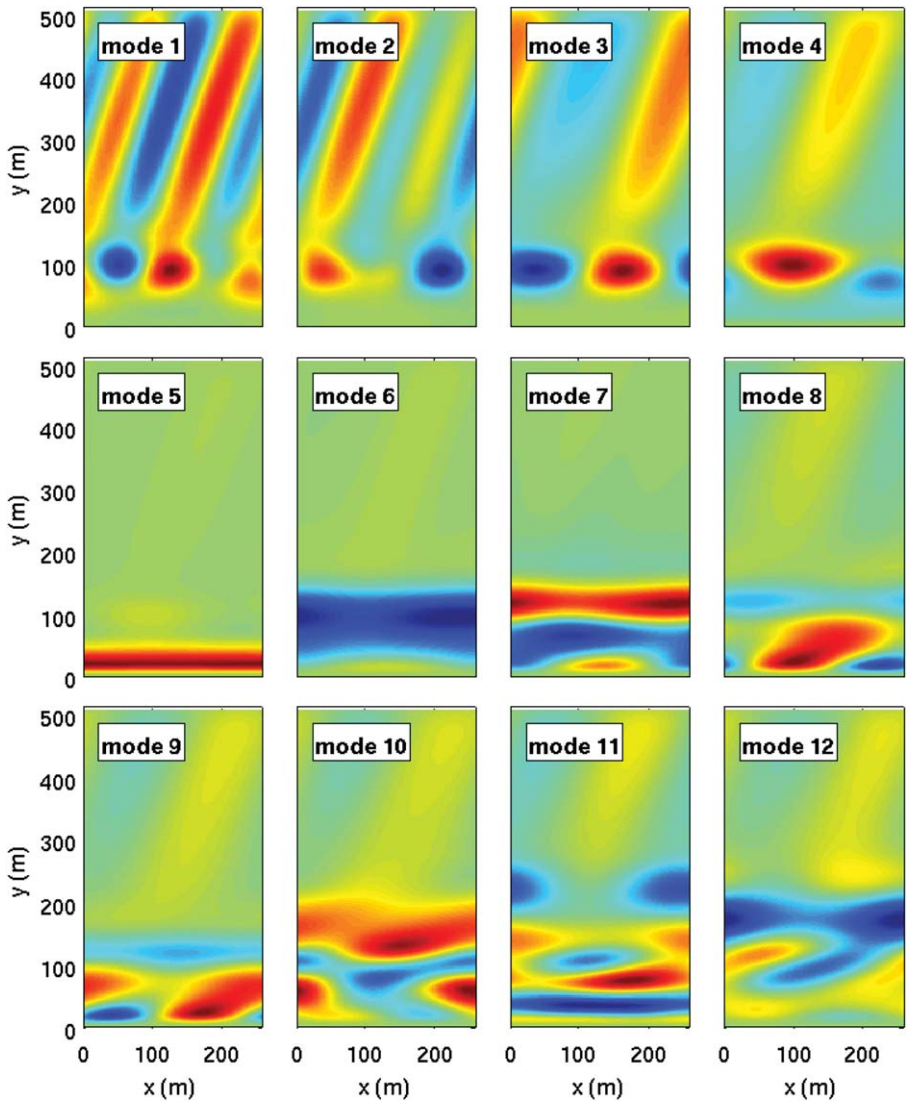

Figure 14. Bathymetry correction functions corresponding to the first 12 array modes.

only 18 modes satisfy this requirement. The bathymetry correction structure corresponding to each of these modes is obtained as $\sum_{k=1}^{K} U_{ki}\delta h_k$, where i is the mode number (Figure 14). In the first four of these most stably observed structures, correction in the area of the bar is strongly coupled with that in the area not covered by the data. These four modes would be stably constrained even in the case of very imprecise data (e.g., with $\sigma_d = 0.2$ m s^{-1}, see Figure 13). Mode 5–8 bathymetry correction structures are locally intensified in the area of the bar and onshore of it. Higher modes are responsible for correction on smaller spatial scales, which exhibit some weak coupling with the distant correction farther offshore.

[38] The fact that only a handful of the model modes can be effectively corrected encouraged us to explore how effective assimilation may be with smaller data sets. These additional observational arrays and posterior bathymetries resulting from their assimilation are shown in Figures 15d–15f. For reference, the true and prior bathymetries are also shown in Figures 15a and 15b. These results correspond to the weakly nonlinear case. In all the cases, the (u,v) data are sampled at points on regular grids, which differ in the offshore extent (Y) and the distance between the data points in each direction (DX). These assimilation cases are labeled as Y-DX; for instance case 256-10 (Figure 15c) is one of the initial cases presented earlier. The inverse bathymetry estimates for each of the cases are presented in Figure 15 and the corresponding RMS errors in Figure 16. It turns out that using data only onshore and over the bar and discarding the points at $y > 128$ m (case 128-10, Figure 15d) results in a bathymetry estimate of almost the same (slightly better in terms of RMS error) quality as the initial case 256-10. Sampling the velocities every 20 m (instead of originally 10 m) in the same smaller area (case 128-20, Figure 15e) degrades the result of the inversion, although this estimate is still a substantial improvement compared to the prior. Case 64-10, using a dense set of data only onshore of the bar trough (Figure 15f), results in an estimate of h that is improved over the prior, albeit only marginally. In that case, the alongshore variability in the bar shape is improved, but it is not moved toward the shore.

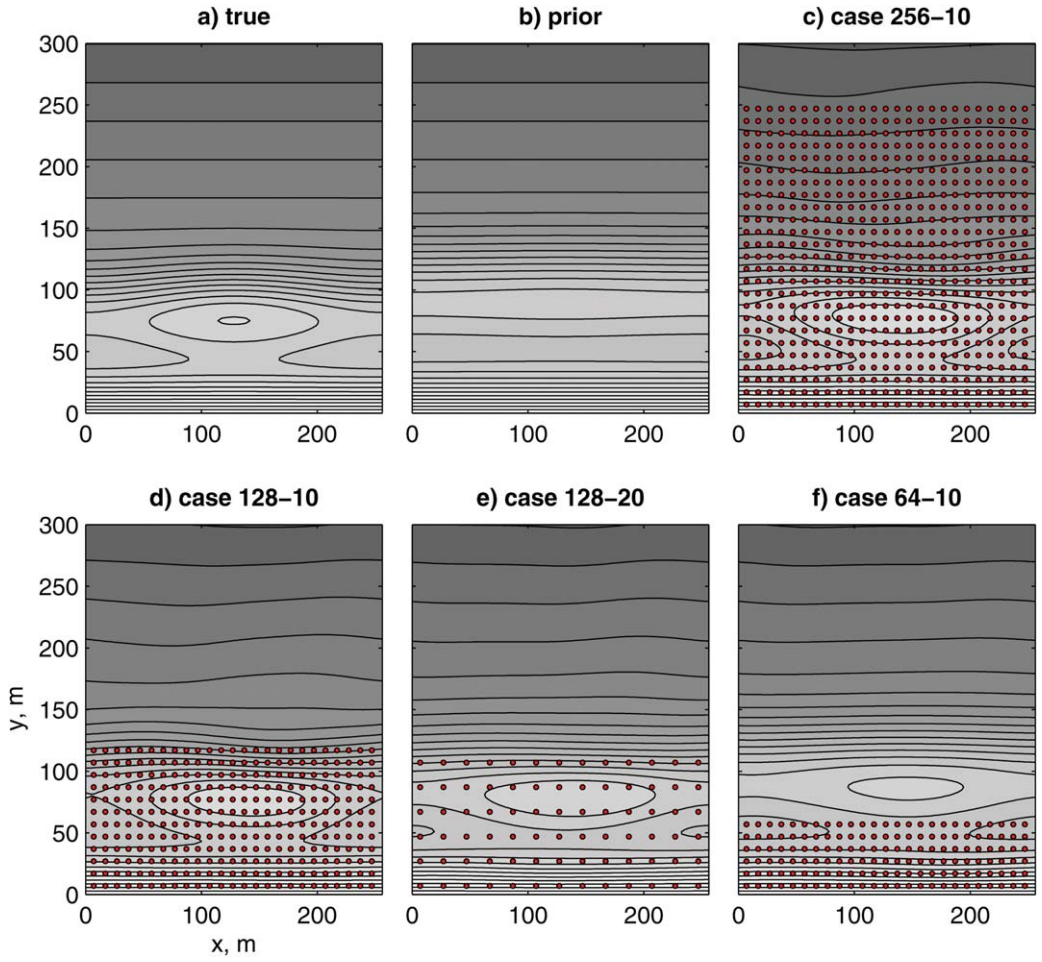

Figure 15. Bathymetries in additional assimilation tests exploring impacts of different data arrays (dots): (a) true, (b) prior, (c) case 256-10 (i.e., data extend to $y = 256$ m, and the distance between data points is 10 m in both alongshore and cross-shore directions), (d) case 128-10, (e) case 128-20, and (f) case 64-10. Bathymetric contours are shown every 0.5 m. RMSE corresponding to these cases is shown in Figure 16.

5. Discussion

[39] In this section some of the model and assimilation method assumptions are discussed in view of the results shown above.

[40] *Özkan-Haller and Li* [2003] showed that alongshore currents may modify the wave field in the nearshore zone, altering the distribution of radiation stresses and affecting stability of the alongshore currents. This feedback mechanism is not included in our forward (nonlinear) model. Although one-way coupling adopted here is certainly an idealization, it captures the essential mechanism of generation of wave-forced alongshore flows and their instabilities. Using such a one-way coupled model is a step toward increasing complexity in the context of variational data assimilation compared to the previous efforts that did not consider model coupling. Using a one-way coupled model compared to a two-way coupled model (in which currents affect waves) offers methodological advantages, demonstrating with great clarity the reversal of the informational flow in the adjoint counterpart of a forward (nonlinear) system, including forcing of the adjoint wave model with sensitivity computed by the adjoint circulation model. As an additional justification to not including the feedback of currents on waves, Froude numbers are generally small and do

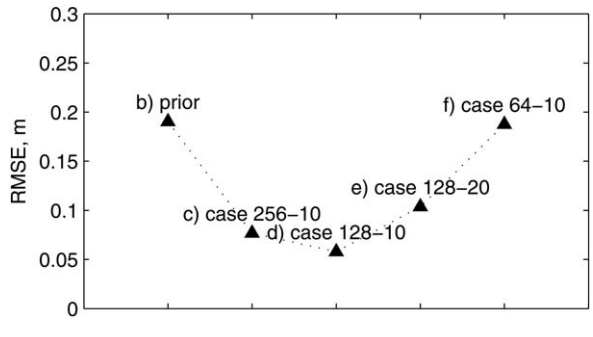

Figure 16. Bathymetry RMSE with respect to the true h, for the cases shown in Figure 15.

not approach unity in this and similar applications [*Wilson et al*., 2013].

[41] For consistency with the assumption of no wetting-drying, the bathymetry error variance was reduced toward the coast. Despite this detail, the variance was nearly constant in the area of the bar where maximum impact on bathymetry was expected. The model error covariance formulation involves several functional forms and parameters. We did not study solution sensitivity to all (or any) of them. The alongshore and cross-shore horizontal decorrelation length scales were chosen to be comparable to the spatial scales in the bathymetry and currents. Those are taken to be sufficiently small. Based on experience, assuming overly long model error decorrelation length scales may degrade the quality of data inversion [e.g., *Kivman*, 1997]. However, it is important to mention that assuming uncorrelated errors (e.g., $C_h = \sigma_h^2 I$, where I is the unity matrix) would yield a singular correction (a linear combination of structures such as that shown in Figure 9).

[42] The correction may also be sensitive to details of the data error covariance. Although we did not investigate this sensitivity, it should be mentioned that processing of the remote sensing data may introduce spatial correlations in errors. Using a diagonal C_d simplifies inversion and is a common practice in data assimilation. Future studies will show how important those details are compared to uncertainties in the choice of C_h.

[43] The array mode analysis suggests a rather limited number of significant orthogonal modes in the bathymetry correction. A possible reason may be a limited alongshore extent of the domain and periodic boundary conditions that constrain alongshore variability in the model. Analysis of the model behavior in a larger domain is a topic of future research. However, we note that advection by a 0.5–1 m s^{-1} alongshore current for a period of 2 hours (the length of the assimilation window) may result in rather long-tailed adjoint sensitivity for a 1 h averaged velocity observation.

[44] Since the manuscript is focused on aspects of assimilation in a coupled model, we do not provide examples of assimilation of wave data. In future studies, it would be interesting to assess the relative impact of assimilation of observed wave parameters and wave-averaged velocities, e.g., using tools developed within the variational formalism [*Moore et al*., 2011b].

[45] Curiously, the case assimilating only the alongshore velocity component worked as well as the case in which both along- and cross-shore components were assimilated (see Figure 16). As a possible explanation, the depth-integrated continuity equation (1) is satisfied exactly. This equation, combined with the no-flow boundary condition, provides a constraint on the cross-shore component of the current given the alongshore currents.

[46] The key result in *Kurapov et al*. [2007] assimilating velocity data in the nearshore circulation model was obtained by building a rather involved error covariance for $\boldsymbol{f}(x,y)$ (see (2)–(3)). We note that in our coupled case, errors in the wave forcing of the circulation model are solely due to errors in h and there is no need to guess the error covariance for $\boldsymbol{f}(x,y)$.

[47] Adjoint sensitivity (Figure 9) and representer fields (Figure 10) can be interpreted as model error covariances. In ensemble-based methods [see *Wilson et al*., 2010] estimation of those can be attempted by averaging over ensembles of model runs. However, because of limited number of elements of these ensembles, long-tail correlations are usually interpreted as erroneous and localization methods are applied to artificially reduce covariances far from observations. Using the variational representer method, we can compute the error covariance fields with long-tail correlations far offshore and provide their dynamical interpretation. Such a result would be analogous to using a representative ensemble of infinitely many model states.

[48] It may be suggested that in the present study, the prior bathymetry is close enough to the truth, such that the method based on linearized dynamics works well. For cases involving larger prior-true differences, the "outer-loop" iterations of the representer method may be used. The inverse bathymetry would be obtained solving a series of linearized problems. On each iteration, the inverse solution from the previous iteration serves as the background state for linearization [*Chua and Bennett*, 2001; *Bennett et al*., 2002; *Kurapov et al*., 2007]. The effectiveness of the nonlinear part of the optimization algorithm in the context of a coupled wave-circulation model is not verified here and is left as a topic of future studies.

6. Summary

[49] Opportunities for bathymetry correction provided by the variational data assimilation method have been explored in the context of a one-way coupled nearshore wave-circulation model. Tests using synthetic data show that assimilation of velocity observations can provide a useful correction to bathymetry. The variational formalism allows separating contributions to bathymetry correction coming directly from the adjoint circulation model and adjoint wave model. In our case, the wave component was responsible for the bar displacement toward the coast and the circulation model for alongshore variability in the bar shape.

[50] Our idealized study discussed advantages of using the variational method, which include a very clear formulation of the optimization problem, a framework for providing bathymetry correction at locations where observations are not available, the possibility to determine contributions from different model components in the coupled system, and the analysis of best constrained spatial structures (array modes). We found that individual representers show local correction as well as correction to bathymetry in areas offshore along the propagation direction of the waves.

[51] Analysis of the array modes suggests that the bathymetric correction can be constrained with relatively few linear combinations of observations. Tests with truncated observational arrays confirm that qualitative and quantitative improvement of the bathymetry can be obtained with observational arrays that mimic those used for remotely sensed (e.g., video-based) surf zone current observations.

[52] Future steps in the direction of using variational methods in the nearshore zone will include the following elements: combined assimilation of wave and circulation data, a wave model describing an evolution of a full spectrum of waves [see *Veeramony et al*., 2010]; a three-dimensional circulation model and its TL and AD components [*Moore et al*., 2011a; *Kurapov et al*., 2011; *Yu et al*.,

2012]; and two-way coupling between the wave and circulation models [*Özkan-Haller and Li*, 2003; *Uchiyama et al*., 2009].

Appendix A: The Wave Model

[53] Here, for reference, the wave model from *Slinn et al*. [2000] is briefly described, taking into account modification (4). Given the root mean square wave height H_{rms} and direction of the incoming waves θ in deep water, these parameters at the offshore boundary of our domain (6.1 m depth) are determined using Snell's law and conservation of wave energy. At any depth, the wave number magnitude $\kappa = (k^2 + l^2)^{1/2}$ is found by inverting the dispersion relation:

$$\omega^2 = g\kappa \tanh[\kappa h] \tag{A1}$$

where, recall, $\omega = 2\pi/T_p$ is the peak wave frequency. Given the conditions at the offshore boundary, (4) is integrated numerically in the direction toward coast using the fourth-order Runge-Kutta method:

$$\frac{\partial k}{\partial y} = \frac{\partial l(k,\omega,h)}{\partial x} \tag{A2}$$

where functional dependency of l on k, ω, and h is defined by (A1). The magnitude of the phase velocity is

$$C = \frac{\omega}{\kappa}. \tag{A3}$$

[54] The magnitude of the group velocity is

$$C_g = \frac{\omega}{2\kappa}\left(1 + \frac{2\kappa h}{\sinh 2\kappa h}\right) \tag{A4}$$

and its components are

$$\begin{aligned} C_g^{(x)} &= C_g \frac{k}{\kappa}, \\ C_g^{(y)} &= C_g \frac{l}{\kappa}. \end{aligned} \tag{A5}$$

[55] To obtain the wave energy $E(x,y)$, the corresponding equation is integrated (from the offshore boundary, using the Runge-Kutta method):

$$\frac{\partial\left(EC_g^{(x)}\right)}{\partial x} + \frac{\partial\left(EC_g^{(y)}\right)}{\partial y} = -\varepsilon_b \tag{A6}$$

where the dissipation function is

$$\varepsilon_b = \frac{3\sqrt{\pi}\rho g B^3}{16 T_p}\frac{H_{rms}^5}{\gamma^2 h^3}\left\{1 - \left[1 + \left(\frac{H_{rms}}{\gamma h}\right)^2\right]^{-5/2}\right\} \tag{A7}$$

$$E = \frac{\rho g H_{rms}^2}{8}. \tag{A8}$$

[56] As in *Slinn et al*. [2000], $B = 1.2$ and $\gamma = 0.43$. The components of the radiation stress tensor are

$$\begin{aligned} S_{xx} &= \frac{E}{2}\left(\frac{2C_g}{C}\cos^2\theta + \frac{2C_g}{C} - 1\right) \\ S_{xy} &= E\frac{C_g}{C}\cos\theta\sin\theta \\ S_{yy} &= \frac{E}{2}\left(\frac{2C_g}{C}\sin^2\theta + \frac{2C_g}{C} - 1\right) \end{aligned} \tag{A9}$$

where

$$\cos\theta = \frac{k}{\kappa}, \qquad \sin\theta = \frac{l}{\kappa}.$$

[57] Finally, the forcing of the momentum equations (2) and (3) is computed as

$$\begin{aligned} f_X(x,y) &= -\frac{1}{\rho h}\left[\frac{\partial S_{xx}}{\partial x} + \frac{\partial S_{xy}}{\partial y}\right], \\ f_Y(x,y) &= -\frac{1}{\rho h}\left[\frac{\partial S_{xy}}{\partial x} + \frac{\partial S_{yy}}{\partial y}\right]. \end{aligned} \tag{A10}$$

[58] **Acknowledgment.** This work was supported by the Office of Naval Research under research grant N00014-10-1–0932.

References

Bennett, A. F. (2002), *Inverse Modeling of the Ocean and Atmosphere*, 234 pp., Cambridge Univ. Press, Cambridge, U. K.

Chua, B. S., and A. F. Bennett (2001), An inverse ocean modeling system, *Ocean Modell.*, *3*, 137–165.

Chickadel, C. C., R. A. Holman, and M. H. Freilich (2003), An optical technique for the measurement of longshore currents, *J. Geophys. Res.*, *108*(C11), 3364, doi:10.1029/2003JC001774.

Dean, R. G., and R. A. Dalrymple (1991), *Water Wave Mechanics for Engineers and Scientists*, 368 pp., World Sci., Singapore.

Egbert, G. D. (1997), Tidal data inversion: Interpolation and inference, *Prog. Oceangr.*, *40*, 81–108.

Evensen, G. (2007), *Data Assimilation: The Ensemble Kalman Filter*, 208 pp., Springer, Berlin.

Farquharson, G., S. J. Frasier, B. Raubenheimer, and S. Elgar (2005), Microwave radar cross sections and Doppler velocities measured in the surf zone, *J. Geophys. Res.*, *110*, C12024, doi:10.1029/2005JC003022.

Feddersen, F., R. T. Guza, and S. Elgar (2004), Inverse modeling of one-dimensional setup and alongshore current in the nearshore, *J. Phys. Oceanogr.*, *34*, 920–933.

Gallagher, E., S. Elgar, and R. Guza (1998), Observations of sandbar evolution on a natural beach, *J. Geophys. Res.*, *103*(C2), 3203–3215, doi:10.1029/97JC02765.

Giering, R., and T. Kaminski (1998), Recipes for adjoint code construction, *ACM Trans. Math. Software*, *24*(4), 437–474.

Hamill, T. M., Whitaker, J. S., and C. Snyder (2001), Distance-dependent filtering of background error covariance estimates in an ensemble Kalman filter, *Mon. Weather Rev.*, *129*, 2776–2790.

Holman, R., N. Plant, and T. Holland (2013), cBathy: A robust algorithm for estimating nearshore bathymetry, *J. Geophys. Res. Oceans*, *118*, 2595–2609, doi:10.1002/jgrc.20199.

Kivman, G. A. (1997), Weak constraint data assimilation for tides in the Arctic Ocean, *Prog. Oceanogr.*, *40*, 179–196, doi:10.1016/S0079-6611(98)00005-6.

Kurapov, A. L., G. D. Egbert, J. S. Allen, R. N. Miller, S. Y. Erofeeva, and P. M. Kosro (2003), M2 internal tide off Oregon: Inferences from data assimilation, *J. Phys. Oceanogr.*, *33*, 1733–1757.

Kurapov, A. L., G. D. Egbert, J. S. Allen, and R. N. Miller (2007), Representer-based variational data assimilation in a nonlinear model of nearshore circulation, *J. Geophys. Res.*, *112*, C11019, doi:10.1029/2007JC004117.

Kurapov, A. L., G. D. Egbert, J. S. Allen, and R. N. Miller (2009), Representer-based analyses in the coastal upwelling system, *Dyn. Atmos. Oceans*, *48*(1-3), 198–218, doi:10.1016/j.dynatmoce.2008-09-002.

Kurapov, A. L., D. Foley, P. T. Strub, G. D. Egbert, and J. S. Allen (2011), Variational assimilation of satellite observations in a coastal ocean

model off Oregon, *J. Geophys. Res.*, *116*, C05006, doi:10–1029/2010JC006909.

Ménard, R. (2005), The chemistry-forecast system at the Meteorological Service of Canada, paper presented at ECMWF Seminar on Global Earth-System Monitoring, Eur. Cent. for Medium-Range Weather Forecasting, Reading, U. K. [Available at http://www.ecmwf.int/newsevents/meetings/annual_seminar/2005/Presentations/Menard.pdf.]

Moore, A. M., H. G. Arango, G. Broquet, B. S. Powell, A. T. Weaver, and J. Zavala-Garay (2011a), The Regional Ocean Modeling System (ROMS) 4-dimensional variational data assimilations systems: Part I—System overview and formulation, *Prog. Oceanogr.*, *91*, 34–49.

Moore, A. M., H. G. Arango, G. Broquet, C. Edward, M. Veneziani, B. Powell, D. Foley, J. D. Doyle, D. Costa, and P. Robinson (2011b), The Regional Ocean Modeling System (ROMS) 4-dimensional variational data assimilations systems: Part III—Observation impact and observation sensitivity in the California Current, *Prog. Oceanogr.*, *91*, 74–94.

Özkan-Haller, H. T., and Y. Li (2003), Effects of wave-current interaction on shear instabilities of longshore currents, *J. Geophys. Res.*, *108*(C5), 3139, doi:10.1029/2001JC001287.

Slinn, D. N., J. S. Allen, and R. A. Holman (2000), Alongshore currents over variable beach topography, *J. Geophys. Res.*, *105*(C7), 16,971–16,998.

Svendsen, I. A. (2006), Introduction to Nearshore Hydrodynamics, 744 pp., World Sci, Singapore.

Uchiyama, Y., J. C. McWilliams, and J. M. Restrepo (2009), Wave-current interaction in nearshore shear instability analyzed with a vortex force formalism, *J. Geophys. Res.*, *114*, C06021, doi:10.1029/2008JC005135.

vanDongeren, A., N. Plant, A. Cohen, D. Roelvink, M. C. Haller, P. Catalán (2008), Beach Wizard: Nearshore bathymetry estimation through assimilation of model computations and remote observations, *Coast. Eng.*, *55*, 1016–1027.

Veeramony, J., D. Walker, and L. Hsu (2010), A variational data assimilation system for nearshore applications of SWAN, *Ocean Modell.*, *35*, 206–214.

Wilson, G., H. T. Özkan-Haller, and R. Holman (2013), Quantifying the length scale dependence of advection in the surf zone, *J. Geophys. Res. Oceans*, *118*, 2393–2407, doi:10.1002/jgrc.20190.

Wilson, G. W., and H. T. Özkan-Haller (2012), Ensemble-based data assimilation for estimation of river depths, *J. Atmos. Oceanic Technol.*, *29*, 1558–1568.

Wilson, G. W., H. T. Özkan-Haller, and R. A. Holman (2010), Data assimilation and bathymetric inversion in a two-dimensional horizontal surf zone model, *J. Geophys. Res.*, *115*, C12057, doi:10.1029/2010JC006286.

Yu, P., A. L. Kurapov, G. D. Egbert, J. S. Allen, and P. M. Kosro (2012), Variational assimilation of HF radar surface currents in a coastal ocean model off Oregon, *Ocean Modell.*, *86–104*, doi:10.1016/j.ocemod.2012-03-001.